Polymer Dynamics in Hydrogenous Systems by Neutron Reflectivity

A. R. ESKER,[1] H. GRÜLL,[2] S. K. SATIJA,[3] C. C. HAN[4]

[1]Department of Chemistry (0212), Virginia Polytechnic Institute and State University, Blacksburg, Virginia 24061

[2]Philips Research Laboratories, 5656 AA Eindhoven, The Netherlands

[3]Center for Neutron Research, National Institute of Standards and Technology, Gaithersburg, Maryland 20899

[4]State Key Laboratory of Polymer Physics and Chemistry, Joint Laboratory of Polymer Science and Materials, Institute of Chemistry, Chinese Academy of Sciences, Beijing, China, 100080

Received 2 September 2003; revised 6 February 2004; accepted 18 February 2004
DOI: 10.1002/polb.20176
Published online in Wiley InterScience (www.interscience.wiley.com).

ABSTRACT: Neutron reflectivity is a powerful tool for exploring polymer dynamics above the glass-transition temperature at short diffusion times in layered thin-film systems. Recent studies of membrane-mediated interdiffusion in deuterium-labeled systems have shown that ultrathin membranes can track the position of the interface in binary polymeric diffusion couples and also can discriminate between perdeuterated and hydrogenous polymers of the same molecular weight. This report shows that similar dynamic information can be obtained for binary hydrogenous polystyrene (hPS) diffusion couples separated by an ultrathin (6-nm) isopentylcellulose cinnamate (IPCC) membrane on Si wafers (air//hPS/IPCC/hPS//Si, where "//" represents an interface between obviously different phases and "/" represents a dynamic interface between polymeric species). In particular, the air//hPS/IPCC/hPS//Si system provides the same information as perdeuterium-labeled polystyrene (dPS) diffusion couples separated by the same IPCC membrane (air//dPS/IPCC/dPS//Si). This technique has potential applications for the study of confinement effects on thin-film dynamics and macromolecular transport across membranes. © 2004 Wiley Periodicals, Inc. J Polym Sci Part B: Polym Phys 42: 3248–3257, 2004
Keywords: diffusion; LB films; nanotechnology; neutron reflectivity

INTRODUCTION

Neutron scattering and neutron reflectivity (NR) have proven to be powerful techniques for probing the structures and dynamics in organic systems.[1,2] The reason for this success is that, unlike a material's light and X-ray scattering properties, its neutron scattering properties can be controlled through isotopic substitution. For light, in which regions with differences in the optical refractive index give rise to scattering, isotopic labeling only has a small effect on the refractive index. More extremely, X-ray scattering, which is governed by electron density differences that principally scale with atomic numbers, is essentially unaffected by isotopic substitution. With neutrons, the scattering is governed by the coherent scattering length density (SLD) or the coherent scattering length per unit of volume (b/V), a nuclear property,

Correspondence to: A. R. Esker (E-mail: aesker@vt.edu) or H. Grüll (E-mail: holger.gruell@philips.com)

Journal of Polymer Science: Part B: Polymer Physics, Vol. 42, 3248–3257 (2004)

which widely varies across the periodic table and even from isotope to isotope.[3] The most famous example of this is the hydrogen atom, with a negative coherent scattering length ($b_H = -3.74$ fm), and deuterium, with a positive coherent scattering length ($b_D = 6.67$ fm). This allows one to synthetically tune the coherent SLD of polyatomic materials:[1,2]

$$(b/V) = N_A \sum_i \frac{\rho_i}{A_i} b_i \quad (1)$$

where i represents different types of atoms; N_A is Avogadro's number; and b_i, ρ_i, and A_i correspond to the coherent scattering length, mass density, and atomic mass of atom type i, respectively. As SLD is directly related to a material's refractive index for neutrons (n)[1,2]

$$n = 1 - \delta + i\beta \quad (2)$$

with the absorption term β being negligible for most organic materials and δ being equal to $(\lambda^2/2\pi)(b/V)$ (where λ is the neutron wavelength), it is possible to synthetically tune the neutron scattering properties of organic materials. This ability to manipulate scattering via isotopic substitution has allowed researchers using NR to obtain high-resolution (ca. 0.5 nm) information on the interfacial structure of a variety of organic-based systems, such as surfactants,[4] tethered polymer brushes,[5] block copolymers,[6] polymer blends,[7] Langmuir–Blodgett (LB) films,[8] and biological systems.[9]

Although isotopic labeling is important for assessing structure and dynamics[10] by NR, as well as other depth profiling techniques such as nuclear reaction analysis,[11] secondary ion mass spectrometry,[12] and forward recoil elastic scattering,[13] caution must be used, particularly with polymeric samples.[14] Early work with small-angle neutron scattering showed that phase separation could occur between high polymers that only differed in terms of deuterium labeling.[15–18] Similarly, NR studies have shown that mixtures of perdeuterium-labeled and hydrogenous materials form a surface excess of the lower energy species at the surface.[19] More recently, it has been shown that a perdeuterium-labeled polymer can pass through an ultrathin membrane more quickly than a hydrogenous polymer of the same degree of polymerization.[20,21]

The focus of this article is an important set of control experiments for the verification of isotopic effects observed during membrane-mediated polymer interdiffusion experiments.[20,21] In these systems, a trilayer is prepared on Si wafers of the type air//C/B/A//Si, where "//" represents an interface between obviously different phases in the system and "/" represents a dynamic interface between polymeric species. In previous studies, species A has been perdeuterium-labeled polystyrene (dPS), species B has been an ultrathin (ca. 6 nm) crosslinked network of isopentylcellulose cinnamate (IPCC) that serves as a model membrane of biological dimensions, and species C has been either hydrogenous polystyrene (hPS)[20] or dPS.[21] NR has been used to measure the displacement of the membrane from its initial position during quench experiments. These systems share similarities with Kirkendall effect experiments in metallic systems[22–24] and gold marker experiments in polymeric systems[25–30] but also exhibit some significantly different effects.[20,21] New results for films of the type air//hPS/IPCC/hPS//Si are provided and are compared with prior results for the air//hPS/IPCC/dPS//Si and air//dPS/IPCC/dPS//Si systems.

EXPERIMENTAL

Materials

Specific polystyrene (PS) properties (Polymer Laboratories, Inc., and Polymer Source, Inc.)[31] are summarized in Table 1.[32] "k" is used in the table and throughout this article as shorthand notation for kg mol^{-1}. The IPCC used for the membrane was prepared as follows.[33] Isopentyl cellulose [0.5 g; nominal degree of substitution (DS) $\approx$ 2.4][8] was reacted with 1.0 g of pyridine and 1.6 g of cinnamoyl chloride (predominately trans) at 50 °C in 25 mL of freshly distilled tetrahydrofuran for 24 h under argon. The resulting polymer was recovered in water and was reprecipitated twice from tetrahydrofuran into water and twice from chloroform into methanol. The final product was dried *in vacuo* at room temperature overnight to afford 0.33 g of the recovered product (nominal yield = 62%). The ^{1}H NMR (Bruker AC 300-MHz FT spectrometer in 1,1,2,2-tetrachloroethane-d_2 at 100 °C) data were as follows: for the cinnamate side-chain protons^{cn}, δ = 7.7 (d, J = 16 Hz, 1H, H-3^{cn}), 7.5 (m, 2H, aromatic^{cn}), 7.3 (m, 3H, aromatic^{cn}), and 6.4 ppm

Table 1. M_w Values of the PS Samples Used in This Study

	Stated[a]			Measured by GPC[b,d]		
Code	M_w (kg mol^{-1})[32]	M_w/M_n	n_w^c	M_w (kg mol^{-1})[32]	M_w/M_n	n_w^c
40k dPS	40.0	1.02	357	40.2	≤1.03	359
39k hPS	39.0	1.02	375	37.5	≤1.03	361
36k hPS*	36.0	<1.1	346	38.1	≤1.03	367
28k hPS	28.5	1.03	274	28.1	≤1.03	270
27k dPS	27.0	<1.1	241	25.6	≤1.03	229

[a] Polymer Laboratories, Inc. (the sample labeled with an asterisk came from Polymer Source, Inc.).
[b] Measured by Qing Gi at the Virginia Polytechnic Institute and State University by GPC against regular PS standards in *N*-methyl pyrrolidone on a Waters 150C instrument with a differential viscometric detector.
[c] Weight-average degree of polymerization.
[d] The relative error in the measured data is about 4%.

(d, J = 16 Hz, 1H, H-3^{cn}); for the cellulose backbone protons^{bb}, δ = 4.3 (br d, 1H, H-1^{bb}) and 3.9–2.9 ppm (br m, 8H, H-2^{bb} to H-6^{bb} + H-1^{ip}); and for the isopentyl side-chain protons^{ip}, δ = 1.7 (br m, 1H, H-3^{ip}), 1.4 (br m, 2H, H-2^{ip}), and 0.9 ppm (dd, 6H, H-6^{ip}). The hydroxyl groups on the cellulose backbone along with the generally broad polymer peaks complicate the integration of the different side groups for an NMR-based DS; therefore, the number of equivalent protons per position on each group is reported. For the same reason, elemental analysis was instead used to calculate the DS (C, 66.13%, and H, 9.46%). Thus, the calculated DS values are 2.1 (isopentyl), 0.3 (cinnamate), and 0.6 (hydroxyl) per monomer, giving a repeat unit molar mass of 347.8 g mol^{-1}. PS equivalent molar masses, which were determined on a Millipore–Waters 860 gel permeation chromatography (GPC) system in tetrahydrofuran, yielded a weight-average molecular weight (M_w) of 176 kg mol^{-1} and a polydispersity index [weight-average molecular weight/number-average molecular weight (M_w/M_n)] of 1.96.

Si Wafer Preparation

The 3-in., 3-mm-thick Si wafers (Polishing Corp. of America, Inc.) were treated with an ozone plasma (Anatech, Ltd.). Plasma cleaning was followed by the boiling of the wafers in a 1:1:5 (v/v/v) mixture of concentrated ammonia, 30% hydrogen peroxide, and deionized water for 1.5 h and in a 7:3 (v/v) mixture of concentrated sulfuric acid and hydrogen peroxide for 1.5 h to create a very hydrophilic Si wafer. Finally, the wafers were exposed to a buffered hydrofluoric acid etch [Complementary Metal Oxide Semiconductor (CMOS)-grade; Doe and Ingalls] for 5 min and to a 40% ammonium fluoride solution (CMOS-grade; Doe and Ingalls) for an additional 5 min to produce a stable hydrophobic surface.

Preparation of the Bottom PS Layer of the Air//C/B/A//Si Trilayer Samples

With a wafer prepared as previously described, an approximately 50-nm-thick layer of PS (polymer A) was prepared via the spin-coating of a filtered (0.25-μm Teflon) PS solution in toluene. Subsequently, the film was annealed for 2 h at 120 °C to ensure the removal of the solvent.

LB Transfer of the Membrane in the Air//C/B/A//Si Trilayer Samples

With the aforementioned annealed PS-coated Si wafers, an approximately 6-nm-thick membrane (B) of IPCC was LB-transferred onto A (air//A//Si). This step was accomplished by the Y-type deposition of six layers at a surface pressure of 15 mN m^{-1} and a dipping speed of 5 mm/min with a NIMA 611 alternating-layer trough (NIMA Technology, Ltd.).

Crosslinking of the Membrane in the Air//C/B/A//Si Trilayer Samples

The membrane was subsequently photocrosslinked in a Ziploc sandwich bag under argon with a mercury lamp (model 90-0003-01, BHK, Inc.) equipped with a 290-nm cutoff filter (Schott Glass Technologies, Inc.) for 10 h at a distance of 5 in. to form a

network and guard against crosslinking of the PS underlayer. By following this procedure, we could wash away the PS layer with $CHCl_3$ after exposure. This observation suggests there was no significant crosslinking of the PS layer during exposure. Preliminary crosslinking experiments for this IPCC sample following established procedures[34] for LB films prepared on hydrophobized quartz substrates in air revealed a maximum conversion to the cycloaddition product of about 20%. This value corresponds to a maximum crosslinking density of one crosslink per 15 monomers. As the major limitation to crosslinking is the mobility of the side chains and the proximity of additional crosslinking groups, similar values should be observed for the crosslinking conditions used in this study. Crosslinking tests for pure IPCC films on Si wafers followed by $CHCl_3$ extraction produced insoluble films of identical thickness for both the model studies and the procedure used in this report. Moreover, the crosslinking density does not seem to be a major factor in the membrane-mediated interdiffusion studies, as similar results were seen for noncrosslinked samples.

In addition to the aforementioned precautions, some simple testing of the effect swelling had on the IPCC membrane layer was also performed. Bilayer samples consisting of air//IPCC (40 nm, crosslinked and noncrosslinked)/dPS (1.4 k, 100 nm, prepared by Jimmy Mays at the University of Tennessee)//Si were prepared. The samples were then annealed as a function of temperature from 50 to 160 °C. For the temperature range of 50–140 °C, NR experiments revealed a gradual increase in the interfacial width from 2 to 15 nm. Between 140 and 160 °C, there was a sharp increase in the interfacial width along with the onset of macroscopic cracking of the crosslinked network. Similar bilayer experiments with the 40k dPS sample used in this study revealed smaller interfacial widths, as expected. On the basis of these control experiments and the fact that all annealing was carried out *in vacuo*, the membranes are believed to be thermally and mechanically stable for annealing at 120 °C, as done in this study.

Preparation of the Top PS Layer of the Air//C/B/A//Si Trilayer Samples

Polymer C, a second PS sample, of a thickness $70 < d\ (\text{nm}) < 90$, was then floated on top of membrane B to form a trilayer. The 70–90-nm-thick film of polymer C was prepared via the spin coating of a filtered (0.25-μm Teflon) PS solution onto a hydrophilic Si wafer. The wafer was prepared as described previously, but it was not exposed to hydrofluoric acid or an ammonium fluoride solution to retain a hydrophilic surface. Deionized water (Nanopure system, Barnstead) was used to lift the spin-coated film C from the hydrophilic wafer, and the hydrophobic Si wafer containing polymer A and the membrane B was used to pick up the floating polymer film C from the water surface. The final trilayer film was then dried for at least 2 h at 80 °C *in vacuo* to remove residual water.

NR Measurements

NR experiments were carried out on the NG7 reflectometer at the National Institute of Standards and Technology Center for Neutron Research. The instrumental resolution ($d\mathbf{q}/\mathbf{q}$), wavelength (λ), and accessible range of the scattering wavevector [$\mathbf{q} = (4\pi/\lambda) \sin \theta$, where θ is the incident angle] were approximately 0.045, 0.475 nm, and 0–2.4 nm^{-1}, respectively.

NR Data Analysis

NR experiments on the trilayers provided unambiguous values of the initial dPS layer thicknesses because of the large SLD contrast between dPS and the hydrogenous materials. Additionally, the layer thicknesses were measured by X-ray reflectivity (XR) to provide consistency checks. XR measurements were carried out on a modified diffractometer (Scintag, Santa Clara, CA) with Cu Kα radiation with a wavelength of 0.1542 nm at the National Institute of Standards and Technology Center for Neutron Research to obtain the initial hPS layer thickness (when it was the bottom layer) and the total film thickness at the end of the experiment for all films.[35] Similarly, XR was used to test several wafers possessing six IPCC layers on spin-coated PS films. These measurements always gave values of 5.7 ± 0.1 nm or 0.95 nm layer^{-1}, which was consistent with published results.[8] This information was consistent with quantitative LB transfer of the IPCC onto the PS-coated surface of the Si wafer. Additionally, the XR results provided an independent check of the standard multilayer fitting routine[36] used for modeling the NR data.

Quench Experiments

The trilayer samples were stepwise annealed at 120 °C, which was 20 K above the glass-transition

temperature (T_g) for PS ($T_g \approx 100$ °C), in a preequilibrated vacuum oven; this allowed the two polymers to interdiffuse through the membrane. After a sample was removed from the oven, nearly instantaneous quenching of the system to room temperature ($<T_g$) was achieved on a 0 °C aluminum block that arrested the interdiffusion process for depth profiling by NR. Quenching below T_g was required as NR experiments took 0.5–4.5 h per sample, the time depending on the volume fraction of deuterium-labeled species in the sample and the spacing between data points required to resolve the features in the NR profiles.

RESULTS

Characterization of the Initial State

Figure 1 shows plots of the reflectivity [$R(\mathbf{q})$], which is the number of reflected neutrons divided by the number of incident neutrons, as a function of $\mathbf{q}$ along with plots of the SLD (b/V) as a function of depth (d) from the air interface for three representative samples: (I) air//dPS (27 k)/IPCC (5.7 nm)/dPS (40 k)//Si, (II) air//hPS (39 k)/IPCC (5.7 nm)/dPS (40 k)//Si, and (III) air//hPS (28 k)/IPCC (5.7 nm)/hPS (36 k)//Si. The three SLD profiles show a dip for the membrane as $(b/V)_{dPS} \gg (b/V)_{hPS} > (b/V)_{IPCC}$. All three samples have slightly different total trilayer thicknesses between 125 and 155 nm, whereas the bottom layer thickness is fairly uniform with $d \approx 50$ nm. The membrane layer thickness, 5.7 nm, is identical for all three systems. The reflectivity profiles have dramatically different features arising from different isotopic labeling. As eq 2 shows, the refractive index for neutrons is less than one for normal materials. Hence, all samples exhibit total reflection of all neutrons, $R(\mathbf{q}) = 1$, for values of θ below the critical angle (θ_c). By applying Snell's law, we can define θ_c for small θ values as follows:

$$\theta_c = \cos^{-1}(1 - \delta) \approx (2\delta)^{1/2} \qquad (3)$$

On the basis of eq 3, the shift in θ_c to smaller $\mathbf{q}$ values in the progression of I → III for Figure 1 occurs because $(b/V)_{dPS}$ is greater than $(b/V)_{Si}$ but $(b/V)_{hPS}$ is less than $(b/V)_{Si}$ and $(b/V)_{IPCC}$ is less than $(b/V)_{Si}$. Hence, the critical wavevector ($\mathbf{q}_c$) value observed for the air//hPS/IPCC/hPS//Si samples is essentially just the value for Si. Above $\mathbf{q}_c$, some of the neutrons penetrate the sample, and this results in a drop in $R(\mathbf{q})$. For $\mathbf{q} > \mathbf{q}_c$,

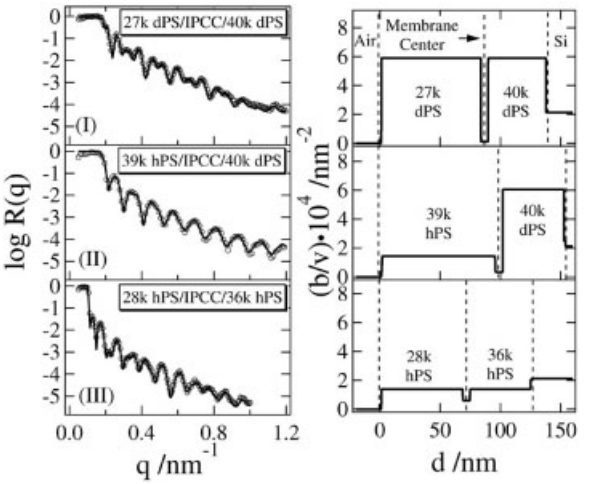

Figure 1. Representative reflectivity and model SLD profiles for the initial states: (I) air//dPS (27 k)/IPCC (5.7 nm)/dPS (40 k)//Si, (II) air//hPS (39 k)/IPCC (5.7 nm)/dPS (40 k)//Si, and (III) air//hPS (28 k)/IPCC (5.7 nm)/hPS (36 k)//Si. The three graphs on the left-hand side show (○) the reflectivity data and (—) the best fits of the data based on the corresponding model SLD profile given to the right. At $\mathbf{q} < 0.8$ nm^{-1}, the standard deviation in the data is smaller than the symbol size. At the highest $\mathbf{q}$ values, the standard deviations correspond to half a decade on a logarithmic scale at most.

there is a dramatic difference in both the magnitude of $R(\mathbf{q})$ and the shapes of the profiles. The overall drop in $R(\mathbf{q})$ for the progression I → III in Figure 1 is due to the loss of strong contrast between the air and polymer at the air/film interface per unit of volume.

Another striking feature of Figure 1 is the difference in the complexity of the $R(\mathbf{q})$–$\mathbf{q}$ profiles. For sample II, there is a simple periodic structure. Periodic oscillations in $R(\mathbf{q})$ or Keissig fringes represent constructive/destructive interference between neutrons reflected from different interfaces within multilayer samples. For I in Figure 1, the complex structure arises from interference between neutrons reflected from the air//dPS, dPS/IPCC, IPCC/dPS, and dPS//Si interfaces. By measuring the spacing between periodic maxima or minima ($\Delta\mathbf{q}$), we can calculate the relevant length scale (L) responsible for a feature from Bragg's law for diffraction that reduces down to

$$L = (2\pi/\Delta\mathbf{q}) \qquad (4)$$

The solid curves in Figure 1 for $R(\mathbf{q})$ versus $\mathbf{q}$ represent results obtained from the fitting of the

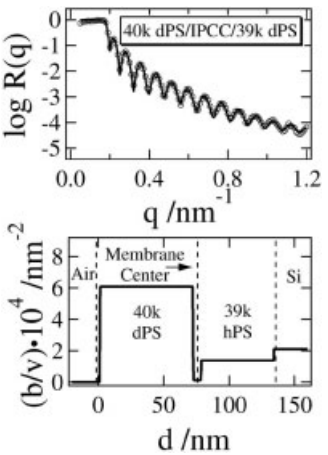

Figure 2. Reflectivity and model SLD profile for the initial state of air//dPS (40 k)/IPCC (5.7 nm)/hPS (39 k)//Si. The top graph shows (○) the reflectivity data and (—) the best fits of the data based on the corresponding model SLD profile given in the bottom plot. At $\mathbf{q} < 0.8$ nm^{-1}, the standard deviation in the data is smaller than the symbol size. At the highest $\mathbf{q}$ values, the standard deviations correspond to half a decade on a logarithmic scale at most.

experimental data according to the SLD profiles with a fitting routine running in Microsoft Excel.[36] Although NR is sometimes criticized as a model-dependent technique for obtaining structural information, the strong interference between neutrons scattered from the different interfaces means that the fits are very sensitive to the membrane position, and this feature essentially eliminates any ambiguity for the membrane position within the trilayer samples. Moreover, with X-ray measurements, and because there is no change in the b/V of the top and bottom layers for dPS/IPCC/dPS or hPS/IPCC/hPS, the models have very few parameters besides the membrane position, thickness, roughness, and composition. Configuration II in Figure 1 leads to a much simpler reflectivity profile. Moreover, a quick calculation of the thickness according to eq 4 shows that the relevant length scale of about 52 nm simply corresponds to the thickness of the dPS layer on the Si substrate. In essence, the low SLD of the hPS and membrane layers makes them nearly transparent in comparison with the dPS layer as strong scattering is only obtained from the IPCC/dPS and dPS//Si interfaces. A similar result is seen if one flips the configuration, air//dPS/IPCC/hPS//Si, an important control done in a previous study,[20] which yields a different $R(\mathbf{q})$ profile, as shown in Figure 2. The reason for the different pattern is that there is now a strong reflection from the air//dPS and dPS/IPCC interfaces, and the dPS layer in Figure 2 is thicker than the dPS layer in Figure 1, configuration II. As a result, the spacing of the features ($\Delta\mathbf{q}$) is consistent with the total film thickness of the floated dPS layer, about 75 nm. Although reflection from the air//hPS and hPS/IPCC interfaces does not significantly contribute to the observed $R(\mathbf{q})$ profile for the initial state, this is no longer the case in the air//hPS/IPCC/hPS//Si samples (configuration III in Fig. 1) because of the absence of a strong scattering layer such as dPS within the trilayer film. Hence, even though air//hPS and IPCC/hPS interfaces weakly reflect neutrons, there is sufficient contrast between them that interference from scattering at the air//hPS, hPS/IPCC, IPCC/hPS, and hPS//Si interfaces significantly contributes to the pattern shown in Figure 1. However, the overall reflected intensity $R(\mathbf{q})$ is lower than that of I and II in Figure 1 or the reversed configuration in Figure 2 because of the overall lower neutron SLD present in the system. The next section examines dynamic studies with configuration III from Figure 1.

Quench Experiments with Air//hPS/IPCC/hPS//Si Films

Interdiffusion commences upon the annealing of the films above T_g of PS. Previous studies of air//hPS/IPCC/dPS//Si and air//dPS/IPCC/hPS//Si samples, in which hPS and dPS had equivalent molecular weights, showed that dPS crossed the membrane more quickly than hPS of equivalent size.[20] Similarly, experiments with air//dPS/IPCC/dPS//Si films showed unequal fluxes of the two layers across the interface for mismatched molecular weights.[21] Figure 3 shows representative raw reflectivity data and fitting results for an air//hPS (28 k)/IPCC/hPS(36 k)//Si film at different annealing times. The SLD models used to fit the data in Figure 3 show that there is a steady migration of the freestanding membrane (the dip in the SLD profile) toward the air interface in the direction of the initially smaller molecular weight species. This observation was expected from previous studies showing how the small-molar-mass species swells the higher molecular weight species.[37] As it is possible to reverse the direction of the motion by the flipping of the configuration with respect to Si and air,[20] the movement of the membrane toward the Si substrate is arbitrarily defined as positive displacement. Figure 4 shows

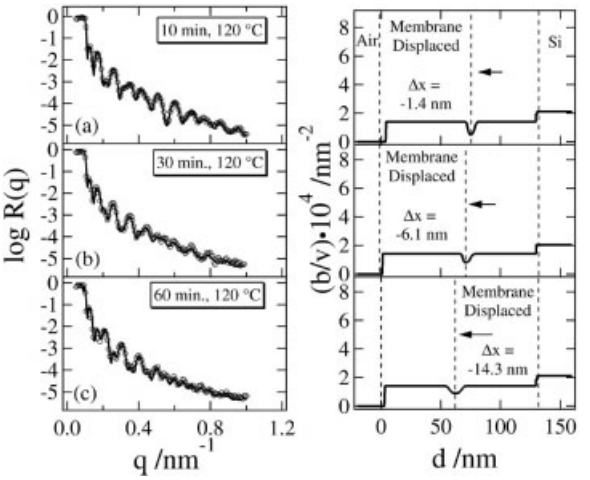

Figure 3. Representative reflectivity and model SLD profiles for air//hPS (28 k)/IPCC (5.7 nm)/hPS (36 k)//Si at three annealing times. The three graphs on the left-hand side show (○) the reflectivity data and (—) the best fits of the data based on the corresponding model SLD profile given to the right for (a) 10, (b) 30, and (c) 60 min of annealing at 120 °C. At $\mathbf{q} < 0.8$ nm^{-1}, the standard deviation in the data is smaller than the symbol size. At the highest **q** values, the standard deviations correspond to half a decade on a logarithmic scale at most. The graph clearly shows the displacement of the membrane (the dip in the SLD) toward the air interface.

the membrane displacement (Δx) as a function of the annealing time (t) for three different hPS/IPCC/hPS pairs. The results show that the absolute values of the rates ($d\Delta x/dt$, initial slopes) and final displacements of the membrane (plateaus) increase in magnitude as the difference in the molecular weight between the top and bottom layers grows. Through the careful selection of the thicknesses of the layers, it is possible to avoid a situation in which the membrane hits the air//film interface or the Si substrate, as might occur if the differences in the molecular weight between layers A and C were too great. As long as Δx is not influenced by the air or Si interfaces, the final displacement of the membrane serves as a sensitive measure of both isotopic and molecular weight effects on membrane-mediated interdiffusion. Figure 5 shows the final membrane displacement (Δx_f) plotted as a function of the difference in the weight-average degree of polymerization (ΔP) for the series of air//hPS (variable)/IPCC (5.7 nm)/hPS (36 k)//Si samples. Data for sets of air//hPS (variable)/IPCC (5.7 nm)/dPS (40 k)//Si and air//dPS (variable)/IPCC (5.7 nm)/dPS (40 k)//Si samples[21] are also included in Figure 5 for comparison. Figure 5 shows linear relationships between Δx_f and ΔP for all three configurations. The air//hPS/IPCC/hPS//Si data nicely agree with the air//dPS/IPCC/dPS//Si samples and produce identical slopes within the experimental error. This result indicates that the slope of the Δx_f–ΔP plot solely provides information about the molecular weight contribution toward Δx. Looking at the air//hPS (variable)/IPCC (5.7 nm)/dPS (40 k)//Si data, we find that the slope is the same, indicating the same molecular weight dependence, but the x-axis intercept is shifted considerably, revealing membrane displacement from its initial position for matched molecular weight species. This shift implies that an isotopic effect is present in the air//hPS/IPCC/dPS//Si systems.

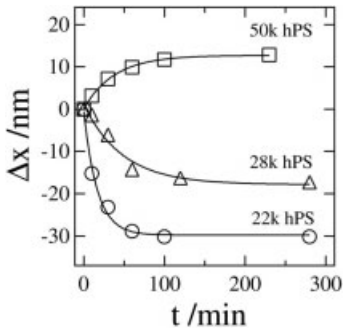

Figure 4. Kinetics of membrane displacement with air//hPS (variable, as indicated on the graph)/IPCC (5.7 nm)/hPS (36 k)//Si. The maximum error for the membrane position is about ±2 nm. The kinetics of membrane displacement can be fit by a single exponential function: $\Delta x = a + b \exp(-ct)$.

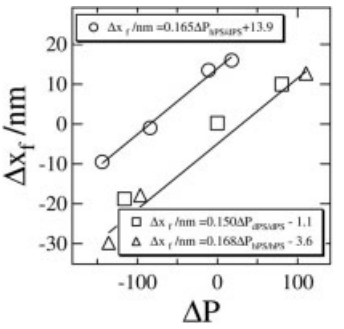

Figure 5. Δx_f as a function of the difference in ΔP between (△) the top polymer layer (B) of variable P and the reference bottom layer [A = hPS (36 k)] with P = 358. Data are also shown for (○) air//hPS (variable)/IPCC (5.7 nm)//dPS (40 k)//Si and (□) air//dPS (variable)/IPCC (5.7 nm)//dPS (40 k)//Si. The fitting line for the dPS/dPS data has been omitted for clarity.

DISCUSSION

Significance of Membrane Displacement

Differences in the chemical potential ($\Delta\mu$) between the upper and lower layers drive interdiffusion through a freestanding membrane.[38,39] The displacement of the freestanding membrane shown in Figure 3 arises from unequal fluxes, $j_i = M_i \times \nabla\mu_i$,[39] where M_i is the Onsager transport coefficient of species i. Assuming a solution–diffusion model, we can break up the mechanism for polymer transport across the membrane into three steps: (1) polymer sorption onto the membrane, (2) polymer diffusion through the membrane, and (3) polymer desorption from the membrane on the opposite side. For a solution–diffusion model, the membrane permeability can be defined as the product of the solubility coefficient and diffusion coefficient ($P = S \times D$). For air//hPS/IPCC/hPS//Si films, the solubility of the different hPS samples used will not vary greatly over the limited molecular weight range examined. However, there will be a substantial difference in the tracer diffusion coefficients, at least 20% for the smallest hPS sample in comparison with 36 kg/mol hPS under the assumption of nonentangled dynamics, and this difference will be greater for the highest molecular weight sample. Hence, differences in the tracer diffusion coefficients drive membrane displacement for the air//hPS/IPCC/hPS//Si films. Figure 5 shows that for each unit difference in the number of repeating units between polymer A and C, the membrane will move by 0.16 nm for the layer thicknesses used in this study. In this respect, the displacement of the interface is reminiscent of the Kirkendall effect experiment, in which oxide impurities present at the interface of a metallic diffusion couple allow one to track the position of the interface,[22–24] and the use of vapor-deposited gold marker experiments in polymer systems allows one to track the position of the interface.[25–30] As similar results have been found for the air//dPS/IPCC/dPS//Si films, one may erroneously conclude that the IPCC membrane serves as nothing more than a sensitive marker for NR experiments. The other line in Figure 5 tells a different story.

Isotope Effects

The air//hPS/IPCC/dPS//Si systems in Figure 5 provide an important contradiction to the marker experiments. In particular, the system air//hPS (39 k)/IPCC (5.7 nm)/dPS(40 k)//Si should possess equal tracer diffusion coefficients for hPS and dPS ($D_{\mathrm{hPS,tracer}} = D_{\mathrm{dPS,tracer}}$). Under these conditions, both the Kirkendall experiments[22–24] and inert gold particles used in polymer systems[25–28] would lead to a stationary interface. The fact that the IPCC membrane moves means that the membrane is not inert and that the phenomenon studied here is fundamentally different from classical marker experiments. In effect, the crosslinked IPCC is functioning as an isotope-selective membrane.

The origin of the isotopic effect in the membrane system appears to be the collective contribution of small differences in the polarizability and molar volume between C—H and C—D bonds to create a slightly positive monomer–monomer interaction parameter (χ_{AB}).[15] As the membrane system has a ternary phase diagram, the relevant interactions are between IPCC, dPS, and hPS. In terms of pairwise interaction parameters, this reduces to χ_{IPCChPS}, χ_{IPCCdPS}, and χ_{hPSdPS}. Literature results for dPS and hPS show that χ_{dPShPS} can be estimated to be approximately 2×10^{-4} at 120 °C.[15] Decreasing entropies of mixing with increasing polymer molecular weight are reflected in the expression of the critical value of the interaction parameter: $\chi_{\mathrm{AB,c}} = 0.5(n_A^{-1/2} + n_B^{-1/2})^2$. For this case, the weight-average degrees of polymerization are $n_{\mathrm{A}} = 359$ and $n_{\mathrm{B}} = 361$ for matched dPS and hPS, respectively, and $\chi_{\mathrm{AB,c}}$ is equal to $0.5(n_A^{-1/2} + n_B^{-1/2})^2 \approx 6 \times 10^{-3}$.[40] Hence, $\chi_{\mathrm{AB,c}}$ is at least larger by a factor of 10 than the estimated value of χ_{dPShPS}, and this indicates that the system is far above its upper critical solution temperature and well inside the one-phase region of the phase diagram. Although the effects on the dPS/hPS interactions are negligible, it is reasonable to conclude that χ_{IPCChPS} is not equal to χ_{IPCCdPS}, which reflects differences in monomer–monomer interactions between hPS and IPCC and between dPS and IPCC. The difference in χ_{AB} upon isotopic labeling then results in a greater dPS flux through the IPCC membrane for the matched molecular weight case. This conclusion is consistent with shifts seen in the phase diagrams of blends between other polymer pairs, such as PS and poly(vinyl methyl ether) upon the isotopic labeling of PS.[41] Even though χ_{AB} can depend on the molecular mass,[42] the predominant effect arises from the chemical groups present in the monomer structure. Hence, it is reasonable to assume that the magnitude of

$\chi_{IPCChPS}$ and $\chi_{IPCCdPS}$ will be retained for different molecular masses even down to monomer sizes. Precedence for isotopic effects on transport processes can also be found in studies of small-molecule systems.[23,43,44]

Advantages of Isotopic Labeling for NR

Given the fact that isotopic labeling can alter the thermodynamics and dynamics of a system, a fair question would be, "Why use isotopic labeling at all for NR experiments?" For structural studies, an obvious reason would be the ability to see a specific part of a molecule or surface. Partial deuterium labeling of surfactants,[4] block copolymers,[6] and polymer blends[7] allows one to determine which part of a molecule adsorbs to a surface, the existence of lamellar ordering, and surface segregation of different components at a surface, respectively. For dynamic experiments, there are three main reasons. The first is that interactions between diffusants and markers, which are often assumed to be inert, can influence the property being measured. As shown previously, the membrane does in fact show differential permeabilities for dPS and hPS, whereas recent studies have suggested that interactions between gold nanoparticles and polymers alter the dynamics of both the polymers and the nanoparticles.[29,30] The second reason is that with isotopic labeling of one component without a marker, it is possible to study the early interdiffusion between two polymers in a bilayer film. Previous studies used this approach to show that the interface does not move without the IPCC membrane.[21] Moreover, the use of isotopic labeling in NR as well as other techniques allows one to deduce the interdiffusion coefficient directly from the data through the diffusion equation[10] in contrast to marker experiments.[25–28]

The final reason for using isotopic labeling is time constraints. The signal-to-noise ratio in NR depends on the square root of the number of reflected neutrons counted. Hence, a practical cutoff for the level of error stated in the figure legends is 100 reflected neutrons. Figure 6 shows the final states after annealing for the same samples shown in Figure 1. As shown in Figure 6, the density of data points necessary to resolve the features is the same for all three configurations (I–III), as all three samples have comparable individual layer and overall film thicknesses. However, no data were taken for configuration III for $\mathbf{q} > 1.0$ nm^{-1}. Looking at configuration I and II, we find that $R(\mathbf{q})$ never dips below $R(\mathbf{q}) = 10^{-5}$, yet $R(\mathbf{q})$ for configuration III, air//hPS/IPCC/hPS//Si, falls below 10^{-5} for $\mathbf{q} > 0.7$ nm^{-1}. Hence, 4.5 h was needed for configuration III to measure a single reflectivity profile. In contrast, configuration I only took about 35 min and configuration II took roughly 1 h to obtain the curves shown in Figure 6, even though a wider $\mathbf{q}$ range was probed with respect to configuration III. Thus, even though comparable dynamic information can be obtained with the purely hydrogenous system, the stronger reflection of neutrons from deuterium-labeled materials yields the possibility of obtaining more data with better signal-to-noise ratios and shorter experimental times.

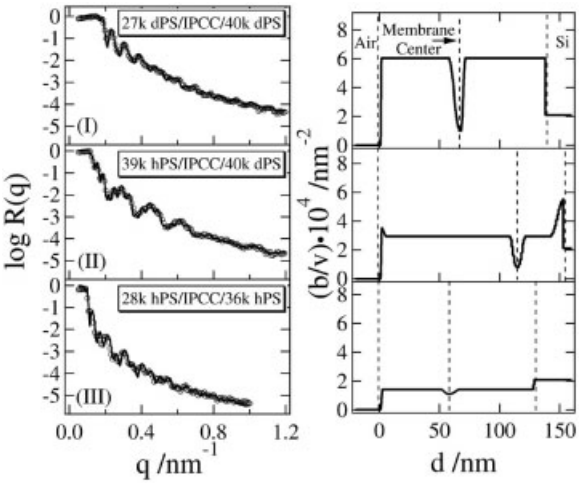

Figure 6. Representative reflectivity and model SLD profiles for the final states: (I) air//dPS (27 k)/IPCC (5.7 nm)/dPS (40 k)//Si, (II) air//hPS (39 k)/IPCC (5.7 nm)/dPS (40 k)//Si, and (III) air//hPS (28 k)/IPCC (5.7 nm)/hPS (36 k)//Si. The three graphs on the left-hand side show (○) the reflectivity data and (—) the best fits of the data based on the corresponding model SLD profile given to the right. At $\mathbf{q} < 0.8$ nm^{-1}, the standard deviation in the data is smaller than the symbol size. At the highest $\mathbf{q}$ values, the standard deviations correspond to half a decade on a logarithmic scale at most.

CONCLUSIONS

NR has been successfully used to study membrane-mediated polymer interdiffusion for hydrogenous systems. These data are consistent with previous studies using deuterium labeling that showed ultrathin IPCC membranes could not be regarded as inert markers and were in fact isotope-selective.[20,21] These studies offer new insight into transport processes across ultrathin barrier layers that may be useful for understanding transport phenomena in

other thin-film[45] and membrane systems of comparable dimensions, such as biological cells[44,46,47] and gas-separation membranes.[48]

Financial support by the Alexander von Humboldt Stiftung and the Thomas F. Jeffress and Kate Miller Jeffress Memorial Trust (J-553) is gratefully acknowledged by H. Grüll and A. R. Esker, respectively. The authors also thank Qing Gi, formerly at the Virginia Polytechnic Institute and State University, for the gel permeation chromatography analysis of the polymers.

REFERENCES AND NOTES

1. Higgins, J. S.; Benoît, H. C. Polymers and Neutron Scattering; Oxford Science: New York, 1994.
2. Russell, T. P. Mater Sci Rep 1990, 5, 171–271.
3. Sears, V. F. Neutron News 1992, 3, 26–37.
4. Lu, J. R.; Su, T. J.; Li, Z. X.; Thomas, R. K.; Staples, E. J.; Tucker, I.; Penfold, J. J Phys Chem B 1997, 101, 10332–10339.
5. Karim, A.; Satija, S. K.; Douglas, J. F.; Ankner, J. F.; Fetters, L. J. Phys Rev Lett 1994, 73, 3407–3410.
6. Mayes, A. M.; Russell, T. P.; Bassereau, P.; Baker, S. M.; Smith, G. S. Macromolecules 1994, 27, 749–755.
7. Grüll, H.; Schreyer, A.; Berk, N. F.; Majkrzak, C. F.; Han, C. C. Europhys Lett 2000, 50, 107–112.
8. Schaub, M.; Fakirov, C.; Schmidt, A.; Lieser, G.; Wenz, G.; Wegner, G.; Albouy, P.-A.; Wu, H.; Foster, M. D.; Majrkzak, C.; Satija, S. Macromolecules 1995, 28, 1221–1228.
9. Majkrzak, C. F.; Berk, N. F.; Krueger, S.; Dura, J. A.; Tarek, M.; Tobias, D.; Silin, V.; Meuse, C. W.; Woodward, J.; Plant, A. L. Biophys J 2000, 79, 3330–3340.
10. Karim, A.; Felcher, G. P.; Russell, T. P. Macromolecules 1994, 27, 6973–6979.
11. Reiter, G.; Steiner, U. J Phys II 1991, 1, 659–671.
12. Schjwarz, S. A.; Wilkens, B. J.; Pudensi, M. A. A.; Rafailovich, M. H.; Sokolov, J.; Shao, X.; Shao, W.; Zheng, X.; Russell, T. P.; Jones, R. A. L. Mol Phys 1992, 76, 937–950.
13. Tead, S. F.; Kramer, E. J.; Russell, T. P.; Volksen, W. Polymer 1992, 33, 3382–3387.
14. Budkowski, A. Adv Polym Sci 1999, 148, 1–111.
15. Bates, F. S.; Wignall, G. D. Phys Rev Lett 1986, 57, 1429–1432.
16. Budkowski, A.; Steiner, U.; Klein, J. J Chem Phys 1992, 97, 5229–5238.
17. Budkowski, A.; Steiner, U.; Klein, J.; Schatz, G. Europhys Lett 1992, 18, 705–710.
18. Klein, J.; Kerle, T.; Zink, F.; Eiser, E. Macromolecules 2000, 33, 1298–1305.
19. Hariharan, A.; Kumar, S. K.; Rafailovich, M. H.; Sokolov, J.; Zheng, X.; Duong, D.; Schwarz, S. A.; Russell, T. P. J Chem Phys 1993, 99, 656–663.
20. Esker, A. R.; Grüll, H.; Wegner, G.; Satija, S. K.; Han, C. C. Langmuir 2001, 17, 4688–4692.
21. Grüll, H.; Esker, A. R.; Satija, S. K.; Han, C. C. Europhys Lett 2002, 57, 533–539.
22. Smigelskas, A. D.; Kirkendall, E. O. Trans Am Inst Miner Eng 1947, 171, 130–142.
23. Tuijn, C. Defect Diffus Forum 1997, 141, 1–47.
24. Morral, J. E.; Son, Y.-H.; Thompson, M. S. Acta Metall 1988, 36, 1971–1975.
25. Kramer, E. J.; Green, P. F.; Palmstrøm, C. J. Polymer 1984, 25, 473–480.
26. Green, P. F.; Palmstrøm, C. J.; Mayer, J. W.; Kramer, E. J. Macromolecules 1985, 18, 501–507.
27. Reiter, G.; Huttenbach, S.; Foster, M.; Stamm, M. Macromolecules 1991, 24, 1179–1184.
28. Liu, Y.; Reiter, G.; Kunz, K.; Stamm, M. Macromolecules 1993, 26, 2134–2136.
29. Cole, D. H.; Shull, K. R.; Rehn, L. E.; Baldo, P. Phys Rev Lett 1997, 26, 5006–5009.
30. Cole, D. H.; Shull, K. R.; Baldo, P.; Rehn, L. Macromolecules 1999, 32, 771–779.
31. Certain commercial materials and instruments are identified in this article to adequately specify the experimental procedure. In no case does such identification imply recommendation or endorsement by the National Institute of Standards and Technology, nor does it imply that the materials or equipment identified is necessarily the best available for the purposes.
32. According to ISO 31-8, the term *molecular weight* (M_w) has been replaced with *relative molecular mass* ($M_{r,w}$). The conventional notation, rather than ISO notation, has been used in this article.
33. Schaub, M. Ph.D. Thesis, University of Mainz, 1993.
34. Iida, S.; Schaub, M.; Schulze, M.; Wegner, G. Adv Mater 1993, 5, 564–568.
35. Anker, J. F.; Majkrzak, C. F. SPIE Proc 1992, 1738, 260.
36. Welp, K. A.; Co, C.; Wool, R. P. J Neutron Res 1999, 8, 37.
37. Composto, R. J.; Kramer, E. J.; White, D. M. Nature 1987, 328, 234–236.
38. Klein, J. Science 1990, 250, 640–646.
39. Kausch, H. H.; Tirrell, M. Annu Rev Mater Sci 1989, 19, 341–377.
40. Nishi, T. J. Macromol Sci Phys 1980, 17, 517–542.
41. Hammouda, B.; Briber, R. M.; Bauer, B. J. Polymer 1992, 33, 1785–1787.
42. Han, C. C.; Bauer, B. J.; Clark, J. C.; Muroga, Y.; Matsushita, Y.; Okada, M.; Qui, T. C.; Chang, T. H.; Sanchez, I. C. Polymer 1988, 29, 2002–2014.
43. Chmielewski, A. G.; Zakrzewskatrznadel, G.; Miljevic, N. R.; Vanhook, W. A. J Membr Sci 1991, 60, 319–329.
44. DeCoursey, T. E.; Cherny, V. V. J Gen Physiol 1997, 109, 415–434.
45. Lin, E. K.; Kolb, R.; Satija, S. K.; Wu, W. L. Macromolecules 1999, 32, 3753–3757.
46. Green, D. R.; Reed, J. C. Science 1998, 281, 1309–1312.
47. Lubensky, D. K.; Nelson, D. R. Biophys J 1999, 77, 1824–1838.
48. Tieke, B. Adv Mater 1991, 3, 532–541.